Fast road detection from color images

Bihao Wang, Vincent Fremont

Fast road detection from color images

Bihao Wang[1,2], Vincent Frémont[1,2],
[1]*Université de Technologie de Compiègne (UTC)*, [2]*CNRS Heudiasyc UMR 7253, France*

***Abstract*—In this paper, we present a method for drivable road detection by extracting its specular intrinsic feature from an image. The resulting detection is then used in a stereo vision-based 3D road parameters extraction algorithm. A substantial representation of the road surface, called axis-calibration, is represented as an angle in log-chromaticity space. This feature provides an invariance to road surface under illuminant conditions with shadow or not. We also add a sky removal function in order to eliminate the negative effects of sky light on axis-calibration result. Then, a confidence interval calculation helps the pixels' classification to speed up the detection processing. At last, the approach is combined with a stereo-vision based method to filter out false detected pixels and to obtain precise 3D road parameters. The experimental results show that the proposed approach can be adapted for real-time ADAS system in various driving conditions.**

***Index Terms*—Road extraction, illuminant invariance theory, drivable space detection**

I. Introduction

Road detection from a driving scene is a popular topic which usually helps the intelligent on-vehicle system to get a better understanding of the environment so that it can improve traffic safety and efficiency. Vision systems constitute key sensors in intelligent vehicles perception task. Their versatility provides rich information like colors, shapes, and depth at low cost with reduced power consumption. Among the popular vision-based researches, road detection not only provide a straightforward information for path planning but also helps to obtain precise obstacle detection and road profile estimation.

Recently, several approaches for image-based road detection have been proposed. In [1], the road detection is performed by boosting image features. In [2], the authors propose to detect the road using a new approach for vanishing points detection combined with texture orientations extraction. In [3], the road detection approach uses Illuminant Invariance Theory on color images to classify road pixels. In [4], the road extraction is based on road borders extraction using texture classification. If the road can be considered as the dominant plane, 3D vision methods like Inverse Perspective Mapping [5], Homography estimation [6], Omnidirectional Images and optical flow [7] or active contours [8], and stereo vision [9], [10], [11].

Basically, the main drawback of vision system, is their sensibility to illumination conditions such as shadows, back-lighting and low rising sun conditions. Especially, shadows are most impactive since they often appear and may lead to false object detection. Thus, road detection in varying illumination conditions becomes a really hard issue, which should be handled with care before further processing.

To solve this problem, [12] presented an impressive method from a view of Invariant Image. Shannon's entropy is used to find and distinguish the intrinsic quality of surface's specular properties. This method has been introduced for road extraction by [3]. In this work, after obtaining intrinsic feature of RGB images, a model-based classifier is built to extract drivable road. Basically, it realizes a simple and efficient separation of road and non-road area from RGB images. But it still remains some drawbacks. For example, it did not avoid the impact of skylight on the axis-calibration result, and the classification threshold value of classifier relies on prior manually segmented ground-truth. From this analysis, we proposed relevant modifications to improve the performance of this algorithm, and we combine the improved method with stereo vision for 3D road plane extraction. Experiments have been taken on different databases and the results proved that our approach is quite fast and robust to be applied for a real-time on-vehicle system.

The rest of this paper is organized as follows. Section 2 briefly recalls the related theory and algorithms. Our proposed approach with theory demonstration and combination with stereo vision are assigned in section 3. Section 4 shows the experimental results. Finally, section 5 concludes this paper and discusses some future works.

II. Related theory

A. Axis-calibration for illuminant invariant images

Shadows often lead to problems in image segmentation and may cause unreliable detection results. According to [12], shadows can be removed by extracting the essential quality of surfaces. Under the assumptions of Lambertian reflectance, approximately Planckian lighting, and fairly narrow-band camera sensors, RGB features of an image captured by camera could be represented as

$$R_i = \sigma E(\lambda_i) S(\lambda_i) q_i \; i = R, G, B \tag{1}$$

Where, σ is a Lambertian shading. $E(\lambda_i)$ is the spectral power distribution; $S(\lambda_i)$ is the surface spectral reflectance function, and q_i is the sensitivity of the camera. The chromaticity is defined as:

$$c_i = R_i / R_3 \tag{2}$$

R_3 represents one channel picked from R,G,B, R_i represent the rest two channels. It is then possible to remove shading

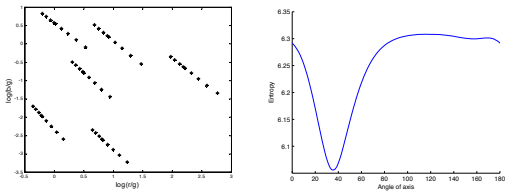

(a) (b)

Figure 1: (a) Example of chromaticities for 6 surfaces under 9 lights in log-chromacity space; (b) Entropy plot for different axis.

information σ and q_i by taking the logarithm of chromaticity:

$$\rho_i \equiv \log(c_i) = \log(s_i/s_3) + (e_i - e_3)/T.\ i = 1, 2 \quad (3)$$

Thus, $\rho_{1,2}$ form a log-chromaticity space (see Fig. 1a). In this space, the pixels on the same surfaces under different illuminations build a straight line. The lines l_i which represent different chromaticities are almost parallel. Their directions are only determined by the factor of $(e_i - e_3)$, which correspond to the spectral power distribution $E(\lambda_i)$. Their displacements $log(s_i/s_3)$ are only related to surface spectral reflectance function $S(\lambda_i)$. Hence, an image I_θ with suppressed shadows can be obtained by projecting the lines l_i on their common orthogonal axis which make an angle θ with the horizontal axis. Therefore, I_θ is lighting independent and is also shadow-free:

$$I_\theta = \rho^T(\cos\theta, \sin\theta),\ \ \rho = (\rho_1, \rho_2) \quad (4)$$

To find the correct axis θ, Shannon's definition of entropy has been introduced:

$$\eta = -\sum P_j(I_\theta) \log P_j(I_\theta). \quad (5)$$

Where P_j is the empirical probability for each bin in histogram of I_θ. The axis that generates a grayscale image with minimum entropy is the correct angle to distinguish different surfaces.

B. Model-based Classification

According to the illuminant invariant property of I_θ, road pixels are expected to be similar regardless of the illumination variety. Therefore, free-road surface and non-road surface could be separated by a model-based classifier as follow [3]:

$$\begin{cases} p \text{ is road}, & \text{if } P(I_\theta(p) \mid \text{road}) \geq \lambda \\ p \text{ is background}, \end{cases} \quad (6)$$

where $P(I_\theta(p)|\text{road})$ represents the probability P of pixel p being on the road according to its illuminant-invariant gray scale value $I_\theta(p)$. λ is a predefined threshold on this measure. $P(I_\theta(p)|road)$ is obtained from a normalized histogram composed of the selected pixels on the road.

The threshold λ is determined by the measurement of detection effectiveness F, where, $F = (2PR)/(P + R)$ with precision P and recall R. The highest effectiveness F gives the desired λ. However, this calculation needs manually segmented ground-truth mask as criterion. Thus, the road-extraction results generated by this method fit to the drivable road area. But, it is difficult to apply it in unknown environments.

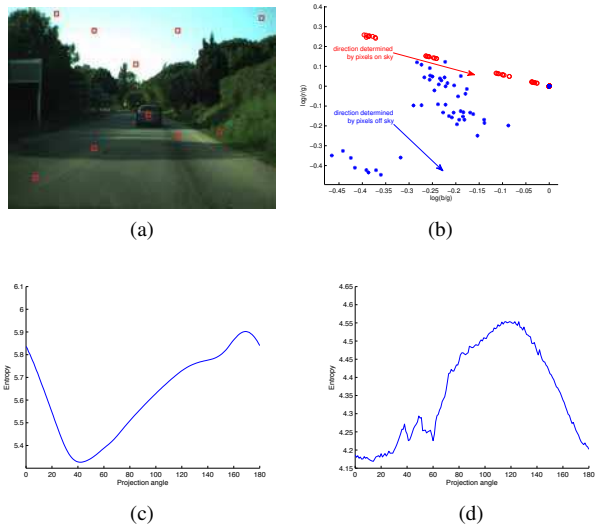

(a) (b) (c) (d)

Figure 2: (a) Samples selected both from sky and other area. (b) Representation of sample pixels transformed in log-chromaticity space, reds are sky pixels and blue the others, arrows are directions determined by these pixels. (c) Entropy plot with sky area taken into consideration. (d) Entropy plot after sky removal.

III. Proposed approach for road detection

Depending on the basic theory and problem analysis, we developed a new method for fast road detection with sustainable modifications and reliable improvements: firstly, sky removal and new log-chromaticity space contribute to the axis-calibration stability and to cost saving; secondly, confidence intervals help in the determination of the threshold λ without any prior knowledge about road conditions; finally, stereo-vision-based extension provides possibility of 3D road profile extraction and improve the detection precision.

A. Sky removal for axis-calibration

Remarkably, axis-calibration results show great variations in Dataset1 (See Section IV A), especially when sky takes more than 30% of the image area. Fig. 2 shows representation differences between sky and real surface. From Fig. 2b, we can get that the pixels from sky do not respect the axis-calibration theory. Indeed, the line formed by them is not parallel to the others in the log-chromaticity space. In fact, the changeful appearance of sky can be explained by Rayleigh scattering:

$$I(\lambda)_{scat} = const \cdot I(\lambda)_{inc}/\lambda^4 \quad (7)$$

I_{scat} represents the intensity of the scattered light. I_{inc} represents the intensity of the incident light, and λ represent the wavelength. Blue color with a small wavelength is more

strongly scattered than red, so it becomes the common color for sky. At sunrise and sunset, the distance from sun to camera is longer, blue is almost scattered away while red is reserved in $I(\lambda)_{scat}$. But for trees and roads, their colors captured by camera are caused by reflection of black-body radiation. This difference tells why axis-calibration theory is not suitable for sky background.

Usually, if the camera is well calibrated, it is possible to determine the horizon line of the images directly. Under this condition, we can simply cut off the above part for sky removal. Else if there is a lack of horizon information, an adaptive horizon finding algorithm mentioned in [13] would be helpful. In this work, the algorithm analyzes the highest 60% area of the image which is divided into 10 parts by empirical horizon line estimation; for each line, an Ostu threshold is calculated, and the most effective value is expected.

To simplify the procedure and to save time, we propose that once the horizon line has been determined at beginning of the sequence, it can be directly applied to the next few images.

Assuming S (sky) and R (road) are two parts separated by determined horizon line, and R', S' represent the two real parts of image. When $R \subseteq R'$, all pixels in R' respect to the same axis θ, so as to R. Else, if $R \supseteq R'$, some sky area is mis-detected as road, noted as $S_{sub} = R - R'$. In practice, slope angles of road are usually smaller than 30 degree while the vertical visual angle of a camera could be from 60 degree to 90 degree. Thus, most of the time, $S_{sub} \ll R'$, then, the influence by S_{sub} is could be neglected. This simplified processing is only used for axis-calibration when the road profile has been extracted. It is then easier to limit the ROI for faster calculation.

B. Log-chromaticity space by geometric mean

After an evaluation of the previous approach, the axis-calibration result still remains unstable. For this reason, we introduced a new log-chromaticity space built by geometric mean to offer an equal processing for R, G, B channel's transformation[12].

From Eq. 2, σ and q_i can be removed through a division by any of the color channels. However, the choice of the denominator is still a tough issue. If the denominator happens to appear rarely in the whole image (e.g. channel red in Dataset1), then the variance of the division would be large [14]. In reality, for long-term driving, the background tonal is changing continuously even dramatically, e.g. an urban scene with colorful buildings along the road. In order to avoid favoring one particular channel, the R, G, B factors could be transformed to division by their geometric mean, i.e

$$C_{ref} = \sqrt[3]{R * G * B} \tag{8}$$

Thus, the definition of chromaticity becomes:

$$c_i = R_i / C_{ref} \tag{9}$$

and the log version remains: $\rho_i = \log(c_i)$. One can notice that in the log space, the color space ρ is orthogonal to $u = 1/\sqrt{3}(1,1,1)^T$.

Therefore, the transformation from the original coordinates to the new geometric mean divided space is:

$$\chi \equiv U\rho, \chi \quad \text{is } 2 \times 1 \tag{10}$$

$U = [v_1, v_2]^T$, and $v_1 = (1/\sqrt{2}; -1/\sqrt{2}; 0)^T$, $v_2 = (-1/\sqrt{6}; -1/\sqrt{6}; 2/\sqrt{6})^T$. Points still retain the parallel lines in the new log space [15]. Then the new shadow-free gray image is calculated by:

$$I_\theta = \chi_1 \cos\theta + \chi_2 \sin\theta \tag{11}$$

Since time consumption of dynamic adjusting method is important, the calibrated angle can be defined off-line, which means the result could be directly used for later varied driving scenes [3]. Thus, as a preparation work, calibration could be realized off-line, and would not affect the real-time detection performance. The algorithm can be summarized as follow:

Algorithm 1 Axis-calibration algorithm

- Determination of the horizon line, cut off above area I_S
- Form a 2D log-chromaticity representation $\chi(I_R)$ for the rest of the image I_R.
- For θ' from 1° to 180° :

1) Form gray-scale image $I_{\theta'}$ by projecting $\chi(I_R)$ to axis θ: $I_\theta = \chi(I_R) \cdot \overrightarrow{\theta}$
2) Forms the histogram of $I_{\theta'}$ with a careful bin-choice and outliers exclusion.
3) Calculate entropy by Eq. 5

- Correct axis θ equals to θ'_{minEnt} which lead to the minimum Entropy.

C. Confidence interval classification

Practical fast road detection should be adaptive to dynamic environment. For this reason, it is necessary to sever the dependency of the prior knowledge about road's ground truth. Based on this consideration, we introduced confidence intervals to determine the threshold λ for the model-based classifier which separates the pixels into road or non-road class.

Notice that, since I_θ has eliminated the influence of shadows, the histogram composed by pixels on road surface is expected to be uni-modal with low dispersion and skewness. Therefore, the normalized histogram follows the empirical form of a normal distribution for a random variable, i.e. $I_\theta(\text{road}) \sim \mathcal{N}(\mu, \sigma^2)$.

Under the assumption that the bottom area of a driving scene image indicates the safe driving distance, as written in [3], a model of road surface could be built with a set of patches dispersed in this area. The representation of the road's illuminant invariance feature can be abstracted from normalized histogram, i.e., $H(I_\theta(p))$, where p represents selected pixels. In this paper, 9 patches with a size of 10×10 at the bottom of images have been devoted to modal construction. With this model, it is easy to calculate statistic parameters μ and σ and to stimulate the distribution of $I_\theta(\text{road})$. Empirically, we believe that the middle 95% data in histogram represents

road's illuminant invariance feature; therefore, we defined confidence level $1-\alpha = 0.95$ to calculate the confidence interval $[\lambda_1 = \mu - 1.86\frac{\sigma}{\sqrt{n}}, \lambda_2 = \mu + 1.86\frac{\sigma}{\sqrt{n}}]$ of $H(I_\theta(p))$.

On the whole image, pixels whose grayscale values fall outside this interval would be regarded as background or obstacles (e.g. vehicles, trees, buildings, etc.). Therefore the classifier could be redefined as:

$$\begin{cases} I_R = 1 \text{ Road}, & \text{if } \lambda_1 \leq I(p) \leq \lambda_2 \\ I_R = 0 \text{ non Road}, & \text{otherwise} \end{cases} \tag{12}$$

Using Eq. 12, we can get a binary images of road detection. This is a rough operation because the threshold is based on a confidence level but may have some pixels be mis-classified. For the false negative pixels we use the operation of holes filling or a 'majority' morphological operation to fix them, but for the false positives, we need fusion information to refine them. That is the purpose of the use of the stereo vision as described in the next section.

Notably, when the vehicle stops right behind the front vehicle, the assumption of bottom road may not stand. In this situation, we record former threshold to estimate the new road condition.

D. Improving road extraction using stereo vision

In past few years, research efforts have been made to use stereo vision in intelligent vehicles applications such as pedestrian detection [16], road extraction [17], etc. A well-known approach in the IV community is the V-disparity approach [18]. In this paper, we applied former method in stereo vision for plane extraction and conversely V-disparity helps to correct the false-detected pixels and even provide depth information of road condition.

With two images of the same scene captured from slightly different viewpoints, disparity map $I\Delta$ could be computed and then it is possible to recover the depth of an object. $I_v\Delta$ is so called the V-disparity image built by accumulating the pixels of same disparity in $I\Delta$ along the v axis [19]. A projected plane in the V-disparity image is usually with the form:

$$\Delta = av + b \tag{13}$$

For different horizontal offsets, their disparities are different. Thus, a surface which is formed by a succession of parts of planes is therefore projected as a piecewise linear curve [20]. Road is modeled as such a plane so that it can be represented by straight slope lines in disparity map and the obstacles on it are represented as vertical lines. In this way, V-disparity approach helps to estimate the longitudinal profile of the road and to detect the presence of obstacles. In this paper, we focus on road profile extraction.

As in common method, all patches on disparity map will be accumulated to compute the V-disparity. However, especially in urban scene, it is hard to define the main line which represents a road area (See Fig.5) with buildings and trees along the road. All these objects will be represented as vertical lines in each distance layout. To solve this problem in our approach, only the pixels that are verified as road area in the binary image I_R could participate in the calculation of the disparity map and in the accumulation for V-disparity. The limitation of ROI of two images will greatly improve the precision of disparity match and reduce the runtime consumption. Reminding that the result of our former processing only gives an extraction of drivable road area, the obstacles (e.g. vehicles and pedestrians) will not be calculated for V-disparity. Thus, a regular sloping line as a representation of the drivable area can be achieved as shown in Fig.5d. According to Eq.13 and applying the Hough transform, the ground plane of image I_G could be constructed by:

$$\text{if}\Delta_{\ p} \in [\Delta_v \pm \varepsilon_v],\ I_G = 1,\ \text{else},\ I_G = 0 \tag{14}$$

Here, we define a dynamic variance $\varepsilon_v = c.v$ which is proportional to v with a constant factor c. We use this parameter because the closer the layout is, the greater the variance becomes.

Finally, we compare I_G and I_R for their intersection to check the road detection result. The algorithm can be summarize as follows:

Algorithm 2 Stereo vision approach for road extraction

1) Compute I_Δ and $I_v\Delta$ with only valid pixels on I_R;
2) Abstract line's function in $I_v\Delta$ with Hough transform;
3) Calculate disparity Δ_v for each horizontal offset v
4) Reconstruct the ground plane area I_G
5) Verify the final detection result:$I_{final} = I_R \cap I_G$

IV. Experimental results

A. Dataset and Processing Platform

The following datasets have been used for evaluation:
Dataset1: Road image database from Computer Vision Center of University Autonoma of Barcelona.
Dataset2: Database of the KITTI (Karlsruhe Institute of Technology and Toyota Technological Institute) Vision Benchmark Suite. Our processing platform is a standard PC with Windows 7 Enterprise OS, with CPU of 2.66 GHz. The computation environment is MATLAB R2012a.

B. Improvement with sky removal

After some tests, the horizon line is basically at 30% top-area in Dataset1. Fig.3a presents an original RGB image from Dataset1, on its right is the axis-calibration result with sky removal. Bottom images in Fig.3 show the comparison between the whole image axis-calibration and sky-removed axis-calibration. In the result of the whole image axis-calibration, the sky pixels become uniform, but shadow remains on the road. After the sky removal, the projection axis of 36° is much closer to the correct axis and shadows are greatly attenuated. As a conclusion, the sky color doesn't follow the rules in Section II, and sky removal can obviously help to correct the result.

In the test of Dataset1, some results are unpleasing. The reason is an over-saturation in some part of the images. When the driving direction is back-lighted, it is hard to capture real colors of the scene. Additionally, some parts without

(a) Original color image

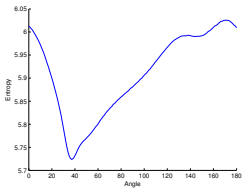

(b) Entropy plot without sky factor

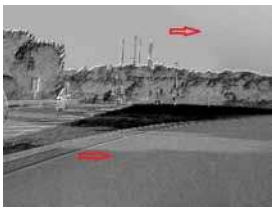

(c) Gray image by whole image axis-calibration

(d) grayscale image get by sky removal axis-calibration

Figure 3: Comparison the gray images got from original algorithm and sky removed algorithm (Dataset1)

illumination may lead to a mixture of self-shadow and cast-shadow which is more complex to separate their optical features.

Dataset	Dataset1		Dataset2	
Measure (log-chroma)	Robust mean	Standard deviation	Robust mean	Standard deviation
Normal	56.3°	17.19°	49.67°	3.88°
Geometric mean	43.4°	16.09°	34.33°	2.17°

Table I: Comparison of normal and geometric mean chromaticities

C. Result in geometric mean divided log-chromaticity

Tab.I compares normal axis-calibration result with only sky removal and the result with modifications of both sky removal and geometric mean division for chromaticity. From this comparison, we can see that the result for geometric mean in 2D space is more stable with a smaller deviation. Fig.4 gives an intuitionist proof of the improvement. We can see that the result for geometric mean in 2D space (Fig.4b) is finer. So the geometric mean division helps to reduce the axis-calibration variance and to improve detection precision.

Additionally, we see that the variance in Dataset1 is much greater than Dataset2, that is because the images of dataset1 contain some special weather and illumination conditions such as cloudy day and over-saturation of the scene.

D. Real-time detection based on confidence interval theory

Modifications based on confidence intervals establish the independency of processing detection with ground truth or temporal constraints. However, the road surface itself also presents some color variations (e.g., worn out asphalt and non-uniformly wet road or the lanes), which may lead to dispersion and noise of the road gray scale. As $\alpha = 0.05$ is just an empirical value for the confidence interval, there must exist deviation from the real situation. Thus, the detection performance may have some wobbles in performance. Hence, we introduced plane extraction based on stereo vision to limit the range of road detection. Conversely the detected area can help to build a clear V-disparity line for 3D reconstruction of the road profile. As to the false negative pixels are excluded by confidence interval, holes filling filters would be useful to fix them.

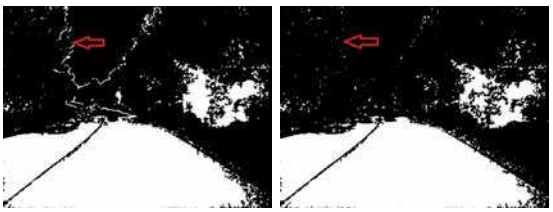

(a) (b)

Figure 4: (a) Primary detection result with only sky removal (b) Primary detection result with both Geometric mean and Sky removal

E. Application to Stereo-Vision Based Road Extraction

In this section we use the Dataset2 which consists of sequences of stereo images of driving scene. Fig. 5 shows improvements with V-disparity estimation: with a limitation of ROI, the line indicating a plane become more clear and precise. Fig. 6 presents the final detection result of our method combining illuminant invariant theory and stereo-vision: the first three images present the results of primary road detection I_R by Alg. 1, plane extraction with constraints of ROI I_G and final detection I_{final} separately. The bottom image presents comparison of final result (red region) with the original RGB image.

The computational cost for primary detection is 1720ms and for stereo-vision-based algorithm is about 1400ms on MATLAB platform with stereo images of size 1242×375. With C++ with optimized code, it is possible to reach about 250ms which corresponds to 4 images per second.

V. Conclusion and Further Discussion

In this paper, we developed a novel method for fast road detection including shadow and sky removals, confidence interval theory and stereo vision detection. The experimental results show that our method provides more stable and more precise results for drivable road detection at a reduced computational cost. The main advantages of our method are: 1. It is simple and can be suitable for real-time and on-line computations; 2. It is independent from prior knowledge of road conditions and temporal constraints. 3. Integration of stereo vision not only improved detection precision but also can provide a reliable platform for obstacle detection with binocular information. From this consideration, our future works will be devoted to the direct use of illuminant invariance theory in the V-disparity calculation in order to get more robust results and to improve

(a) Left image

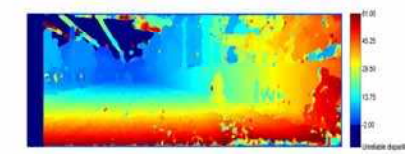

(b) Disparity map of the scene

(c) Classic V-Disparity

(d) Modified V-Disparity

Figure 5: V-Disparities for dataset 3

road obstacle detection. Furthermore, obstacle information can also guide the system to choose proper sample pixels on the road besides the safe driving distance constraint.

REFERENCES

[1] S. Yun, Z. Guo-ying, and Y. Yong. A road detection algorithm by boosting using feature combination. In *Intelligent Vehicles Symposium, 2007 IEEE*, pages 364–368, 2007.

[2] Hui K., J.-Y. Audibert, and J. Ponce. General road detection from a single image. *Image Processing, IEEE Transactions on*, 19(8):2211–2220, 2010.

[3] J.M.A. Alvarez and A.M. Lopez. Road detection based on illuminant invariance. *Intelligent Transportation Systems, IEEE Transactions on*, 12(1):184–193, 2011.

[4] S. Graovac and A. Goma. Detection of Road Image Borders Based on Texture Classification. *International Journal of Advanced Robotic Systems*, 9:1, 2012.

[5] P. Cerri and P. Grisleri. Free space detection on highways using time correlation between stabilized sub-pixel precision IPM images. In *IEEE ICRA*, number April, pages 2235–2240, 2005.

[6] G. Chunzhao, S. Mita, and D. McAllester. Drivable road region detection using homography estimation and efficient belief propagation with coordinate descent optimization. In *Intelligent Vehicles Symposium, 2009 IEEE*, pages 317–323, 2009.

[7] W. Yoshizaki, Y. Mochizuki, N. Ohnishi, and A. Imiya. Free Space Detection from Catadioptric Omnidirectional Images for Visual Navigation using Optical Flow. In *The 8th Workshop OMNIVIS*, 2008.

[8] P. Merveilleux, O. Labbani-Igbida, and E.-M. Mouaddib. Real-time free space detection and navigation using omnidirectional vision and parametric and geometric active contours. In *IEEE ICRA*, pages 6312–6317, 2011.

[9] N. Hautiere, R. Labayrade, M. Perrollaz, and D. Aubert. Road scene analysis by stereovision: a robust and quasi-dense approach. In *Control, Automation, Robotics and Vision, 2006. ICARCV '06. 9th International Conference on*, pages 1–6, 2006.

(a) Primary road detection by Axis-Calibration

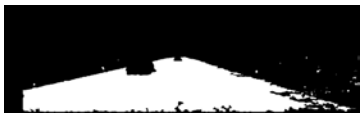

(b) Plane extraction by V-disparity

(c) Final road detection result by fusion processing

(d) Final Road detection result in original image

Figure 6: Road detection with stereo vision

[10] N. Soquet, D. Aubert, and N. Hautiere. Road segmentation supervised by an extended v-disparity algorithm for autonomous navigation. In *Intelligent Vehicles Symposium, 2007 IEEE*, pages 160–165, 2007.

[11] H. Badino, R. Mester, T. Vaudrey, and U. Franke. Stereo-based Free Space Computation in Complex Traffic Scenarios. In *IEEE Southwest Symposium on Image Analysis and Interpretation*, pages 189–192. Ieee, March 2008.

[12] G.D. Finlayson, M.S. Drew, and L. Cheng. Intrinsic images by entropy minimization. In *European Conference on Computer Vision*, 2004.

[13] A.M. Neto, A.C. Victorino, I. Fantoni, and D. E. Zampieri. Robust horizon finding algorithm for real-time autonomous navigation based on monocular vision. In *Intelligent Transportation Systems (ITSC), 2011 14th International IEEE Conference on*, pages 532–537, 2011.

[14] G.D.Finlayson, M.S.Drew, and C. Lu. Entropy minimization for shadow removal. *International Journal of Computer Vision*, 2009.

[15] G. D. Finlayson and Mark Drew. 4-sensor camera calibration for image representation invariant to shading, shadows, lighting, and specularities. In *In ICCV?01: International Conference on Computer Vision*, pages 473–480, 2001.

[16] D.F. Llorca, M.a. Sotelo, a.M. Hellín, a. Orellana, M. Gavilán, I.G. Daza, and a.G. Lorente. Stereo regions-of-interest selection for pedestrian protection: A survey. *Transportation Research Part C: Emerging Technologies*, 25:226–237, December 2012.

[17] N. Soquet, D. Aubert, and N. Hautiere. Road segmentation supervised by an extended v-disparity algorithm for autonomous navigation. In *Intelligent Vehicles Symposium, 2007 IEEE*, pages 160–165, 2007.

[18] Z. Hu and K. Uchimura. U-v-disparity: an efficient algorithm for stereovision based scene analysis. In *Intelligent Vehicles Symposium, 2005. Proceedings. IEEE*, pages 48–54, 2005.

[19] D. Pritchard. Cloth parameters and motion capture. Technical report, 2003.

[20] N. Hautiere, R. Labayrade, M. Perrollaz, and D. Aubert. Road scene analysis by stereovision: a robust and quasi-dense approach. In *Control, Automation, Robotics and Vision, 2006. ICARCV '06. 9th International Conference on*, pages 1–6, 2006.